

Long-term variability of Sea Surface Temperature in the Tropical Indian Ocean in relation to climate change and variability

Soumya Mohan*^{1,2}, Saroj K. Mishra¹, Sandeep Sahany^{1,3}, Swadhin Behera⁴

¹Center for Atmospheric Sciences, IIT Delhi, New Delhi, India

²CSIR-National Institute of Oceanography, Dona Paula, Goa, India

³Centre for Climate Research Singapore, 36 Kim Chuan Road, Singapore

⁴Application Laboratory, Japan Agency for Marine-Earth Science and Technology, Yokohama, Japan

Corresponding Address: Soumya S Mohan

Physical Oceanography Division

CSIR-National Institute of Oceanography

Dona Paula – 403004, Goa, India

E-mail: soumyamohan866@gmail.com

Abstract

The long-term change in the sea surface temperature (SST) of the Tropical Indian Ocean (TIO) and the underlying mechanisms are examined in detail by analysing multiple reanalysis datasets and historical simulations of a global climate model. A robust basin-wide warming signal was found in SST, with the highest long-term warming trend ($\sim 0.09 \pm 0.015^\circ\text{C decade}^{-1}$) seen over the north-western and equatorial Indian Ocean regions. The robust warming trend of TIO SST is a dominant warming signal of the global tropical oceans and is largely in phase with similar warming in western Pacific and Atlantic Oceans. The central equatorial Indian Ocean and south TIO regions went through significant warming during recent decades. The weakened cross-equatorial flow and the associated cyclonic winds over the Arabian Sea region have resulted in equatorial westerlies with an enhanced loss of latent heat over the central and eastern equatorial Indian Ocean. The anomalous cyclonic wind stress curl, in turn, caused mixed layer stratifications in the western Indian Ocean. The advective heat transfer from the south-eastern Indian Ocean to the western Indian Ocean and reduced oceanic cooling by vertical processes, overcome the cooling by the net loss of surface heat fluxes, and favor surface warming the TIO.

Keywords: sea surface temperature, warming, tropical Indian Ocean, mixed layer, wind stress curl, stratification

Highlights

- ◆ The robust basin-wide warming of the TIO is a dominant warming signal of the global tropical oceans and is largely in phase with the warming of the western Pacific and Atlantic Oceans.
- ◆ The cyclonic circulation of the Arabian Sea basin resulted in equatorial westerlies and enhanced latent heat loss over the central equatorial Indian Ocean.
- ◆ The interesting feature of the long-term warming in TIO is that the oceanic processes reinforce the warming tendency, which overcomes the cooling by the net loss of surface heat flux.

1. Introduction

The Indian ocean warming and its teleconnections play a crucial role in the modulation of the global climate system (e.g., Luo et al., 2012; Chen et al., 2019). Since the 1950s, the tropical Indian Ocean (TIO; 30°N-30°S and 30°E-120°E) has warmed faster than elsewhere in the tropical ocean basins (Han et al., 2014) consistent with the global sea surface temperature (SST) trend. The Indian Ocean SST variability has implications on environmental and associated socioeconomic status of the Indian Ocean rim countries. The intensity and distribution of Indian summer monsoon has changed and is projected to change substantially in the future (Sharmila et al., 2015; Sahany et al., 2019; Bhowmick et al., 2019; Mishra et al., 2019). Considering the regional and remote impacts of TIO warming, it is highly desirable to understand the SST variability and change to improve the monsoon predictability (Kucharski and Abid, 2017).

Long-term variations of SST anomaly patterns resulted from a combination of intrinsic modes of atmospheric and oceanic circulation variabilities and coupled ocean-atmosphere interactions (Deser et al., 2010). The SST variability of TIO shows a centennial warming trend superimposed on interannual and decadal variations as well as a rapid warming trend during 2003-2013 (Li et al., 2017). Previous studies (e.g., Li et al., 2016; Han et al., 2014) speculated that the remote forcing from Atlantic and Pacific basins contributes to upper-ocean warming of TIO. However, based on observation and climate model-based analysis, Li et al. (2017) suggested that the tropical ocean basins are tightly connected through multiple atmospheric teleconnections besides the inter-oceanic connection. Atlantic Ocean regional effect can feedback to the Pacific (Kucharski et al., 2015), which influences the Indian Ocean through atmospheric teleconnections (Li et al., 2016).

Previous studies (e.g., Deser et al., 2010; Dong and Zhou et al., 2014) linked the warming of Indian Ocean, especially since the 1950s, to El Niño driven air-sea interactions and greenhouse gas forced radiative and heat flux contributions. Dong and Zhou (2014) showed that anthropogenic forcing contributes to basin-wide warming pattern causing frequent Indian Ocean Dipole (IOD) events. Enhanced wind stress curl in the south Indian Ocean also contributed to the basin-wide warming of the Indian Ocean (Cai et al., 2007). Anthropogenic activities and warming in the Indian Ocean have influenced the Indian summer monsoon (e.g., Singh et al., 2019; Roxy et al., 2014). Hence, a rigorous analysis of SST variability of TIO and its quantification has scientific and societal significance. Our understanding regarding the persistent long-term warming revealed by observations, reanalysis and climate models is less sufficient for reliable future projection and impact assessments. The previous study by Dong and McPhaden (2016) suggested weaker warming over the north tropical Indian Ocean compared to the enhanced warming of southern Indian Ocean (south of 10°S) under the influence of

Pacific heat transport through an inter-oceanic connection. We limit our study domain to TIO to highlight its warming trend and coherency with global tropical oceans. Also, the tropical Indian Ocean warming/cooling is sensitive to Indian summer monsoon variability and is highly significant to the livelihood of the population across the Indian subcontinent.

In this paper, we examine three gridded reanalysis SST data sets available for the period of 1900-2017 to examine the consistency and causes of TIO warming. The study is aimed at addressing the following questions: Is the previously reported Indian Ocean warming trend also prominent over global tropical oceans and is it robust across different SST products? Is the imprint of natural and anthropogenic warming localised in a specific region across different SST products? The study also attempts to understand how the air-sea fluxes and mixed layer heat content of the tropical Indian Ocean are adjusting in a warming climate. A brief description of datasets and methodologies used in the study is given in Section 2. The results and discussions are presented in Section 3, and the results have been summarised in Section 4.

2. Data and Methods

2.1 Data sets

In the present study, five gridded reanalysis SST datasets are considered; the Hadley Center sea ice and SST dataset version 1.1 (HadISST1.1; Rayner et al., 2003), the extended reconstructed SST version 5 (ERSSTv5; Smith and Reynolds 2004; Smith et al., 2008), and the centennial in situ observation-based estimate of SST (COBE-SST2; Hirahara et al., 2014; Ishii et al., 2005). The HadISST ($1^\circ \times 1^\circ$), ERSST ($2^\circ \times 2^\circ$), and COBE ($1^\circ \times 1^\circ$) SST products use different statistical procedures to fill the missing data. The indices of leading climate mode of Indo-Pacific region include Indian Ocean Dipole (IOD; Saji et al., 1999; Webster et al., 1999), El Niño-Southern Oscillation (ENSO; Rasmusson and Carpenter, 1982), ENSO Modoki (Ashok et al., 2007; Ashok and Yamagata, 2009), Pacific Decadal Oscillation (PDO; Mantua et al., 1997) and Atlantic Multidecadal Oscillation (AMO; Schlesinger and Ramankutty, 1994; Enfield et al., 2001) were also considered in the study. The other data sets include monthly surface winds, and air-sea fluxes obtained from National Centers for Environmental Prediction (NCEP) reanalysis (Kalnay et al., 1996; Kristler et al., 2001) for the period 1948-2017. For the estimation of mixed layer heat budget components, sub-surface currents (u , v and w), temperature and salinity fields are obtained from NCEP's Global Ocean Data Assimilation System (GODAS; Behringer and Xue, 2004, Nishida et al., 2011). Since the GODAS products are available only from January 1980, mixed layer heat content and heat budget terms could only be calculated for the period of 1980-2017. We also assessed SST warming and mechanisms using

Community Earth System Model version 2 (CESM2; Hurrell et al., 2013) historical simulations in the phase six of the Coupled model Intercomparison Project (CMIP6; Eyring et al., 2016).

2.2 Analysis methods

2.2.1 SST

The SST data sets with monthly resolution and an overlapping period of 1900-2017 is considered for the present study. We exclude the data before 1900 as the uncertainties in SST data sets are high before then. We interpolated each data set onto a common $1^\circ \times 1^\circ$ grid. Climatological monthly anomalies are subtracted from each grid point for all data sets to obtain SST anomalies. An ensemble mean of SST anomaly is constructed from these three products and consensus in variability among them is examined. Three different periods were considered to analyze the SST trend and variability: period 1 (P1; 1900-2017), period 2 (P2; 1948-2017), period 3 (P3; 1980-2017). The linear trend from the ensemble means SST anomalies are computed using the method of least-squares.

The signal-to-noise maximising empirical orthogonal function (EOF) analysis is an effective method to distinguish between external and natural modes of climate response (Soloman et al., 2011). Hence, we perform low-frequency component analysis (LFC, Wills et al., 2018) based on linear discriminant analysis (an approach is taken from pattern recognition theory), which allows one to distinguish the pattern between natural climate variations and that of anthropogenic forcing (Swanson et al., 2009). A multilinear regression analysis is performed to link SST anomalies with global warming and climate modes to examine the imprints of climate variability and change on TIO warming.

2.2.2 The heat content of the mixed layer

The heat content (H) of the ocean layers between the surface (η) and the depth of the mixed layer (h) is computed as

$$H = \rho C_p \int_h^\eta \theta dz$$

Here, ρ (1025 kgm^{-3}) is the density of seawater, C_p ($4185 \text{ JKg}^{-1}\text{K}^{-1}$) is the specific heat capacity of seawater and θ is the potential temperature of seawater. In this study, mixed layer depth (MLD) is computed based on density (sigma-t) criteria (Lukas and Lindstrom, 1991) that is the depth at which the density (sigma-t) exceeds the surface value by 0.2 kgm^{-3} (Narvekar and Kumar, 2014).

2.2.3 Heat budget of the mixed layer

The SST and ocean mixed layer temperature are tightly coupled and those are generally assumed to be proportional (e.g., Exarchou et al., 2018). Hence, to understand the roles played by air-sea fluxes and oceanic advection on consistent warming of Indian Ocean, we have analysed the mixed layer heat budget (e.g., Vialard and Delecluse, 1998; Rao and Sivakumar, 2000) of the TIO. The conservation of heat in the mixed layer is given by

$$\frac{\partial T_a}{\partial t} = \frac{Q_{net} - Q_{pen}}{\rho C_p h} - \left(u_a \frac{\partial T_a}{\partial x} + v_a \frac{\partial T_a}{\partial y} \right) - \left(\frac{T_a - T_{-h}}{h} \right) \left[W_h + \frac{\partial h}{\partial t} \right] + Residual$$

The heat budget term on the left-hand side represents the mixed layer temperature tendency, and the first three terms on the right-hand side represent the tendency due to net heat flux, horizontal advection and vertical processes. The fourth term, residual (R), represents the tendency due to diffusive heat fluxes the mixed layer and errors. T , u and v denote the temperature and horizontal components of velocity. The suffix a denotes the quantity vertically averaged over the mixed layer and the subscript $-h$ denotes the quantity at the base of the mixed layer. The vertical advection below mixed layer is inferred from the vertical displacement of isotherms in the thermocline (McPhaden and Hayes, 1991). We estimate the vertical velocity W_h as the time rate of change of 20°C isotherm depth (e.g., Alory and Meyers, 2009). This heat budget does not compute diffusion components because of their negligible contribution on a long-time scale. The surface net heat flux, Q_{net} , due to air-sea exchange of fluxes is estimated as

$$Q_{net} = Q_{sw} - (Q_{lw} + Q_{lhf} + Q_{shf})$$

Q_{net} consists of net surface short wave radiation Q_{sw} (positive into the ocean), which warms the ocean surface layers, and non-solar fluxes (positive out of the ocean) of net longwave (Q_{lw}), latent heat (Q_{lhf}) and sensible heat (Q_{shf}). Following Sweeny et al. (2005), we estimate the penetrative loss of shortwave radiation to the oceanic mixed layer Q_{pen} as

$$Q_{pen} = 0.47 Q_{sw} \left[V_1 e^{-\frac{h}{\varepsilon_1}} + V_2 e^{-\frac{h}{\varepsilon_2}} \right]$$

Where ε_1 and ε_2 are the attenuation depths of long visible, short visible and ultra violet wavelengths. We adopt the values of V_1 , V_2 , ε_1 , and ε_2 as 0.39, 0.69, 1.52, and 18.9, respectively as

estimated by previous studies for the Indian Ocean region (Girishkumar et al., 2013; Thadathil et al., 2016). All the estimated heat budget components have been converted to the same unit as the mixed layer temperature tendency ($^{\circ}\text{Cmonth}^{-1}$).

3. Results and discussions

3.1 Long-term warming of tropical Indian Ocean

We consider the ensemble mean SST anomaly obtained from three SST data sets to substantiate the extensively discussed (e.g., Roxy et al., 2014; Dong and McPhaden, 2016) TIO warming. The study examines the SST variability over the 118 years from 1900-2017. However, we also considered the periods 1948-2017 and 1980-2017 to ensure the robustness and to explore the mechanisms of consistent warming of TIO. Figure 1 intercompares the spatial patterns of SST trends in each product and ensemble mean for the TIO region. The spatial trend distribution has been considerably varied over the three different periods and highlights the steady warming of TIO. The differences in the warming patterns across the three different periods indicate multi-decadal variability; and the warming trends are overall consistent across all three datasets. Over the north-western TIO, there is indeed an increase in warming, and $0.09 \pm 0.015^{\circ}\text{C}$ per decade is observed from 1900 to the present. In contrast, the central equatorial Indian Ocean and south TIO regions went through a significant warming rate of $0.16^{\circ}\text{C decade}^{-1}$ and $0.25^{\circ}\text{C decade}^{-1}$ during recent decades. Along the north-western boundary and southern tropical regions, amplitude of SST variability is stronger and relatively weaker in the Bay of Bengal and eastern equatorial Indian Ocean regions indicate a clear east-west difference in north Indian Ocean especially during P1 and P2 (Fig. S2). The spatial patterns of SST climatology (Fig. S1) and standard deviation (Fig. S2) are similar across HadISST, ERSST, and COBE. In the TIO, the regions of SST variations are generally consistent across the reanalysis products considered. Hence, we adopt the ensemble mean SST anomalies to illustrate the significant features of century-long warming of TIO.

The global surface warming during the global warming hiatus period (e.g., Xie and Kosaka, 2017; Liu and Xie, 2018) has slowed down to $0.005^{\circ}\text{Cyear}^{-1}$ (IPCC, AR5; Stocker et al., 2013). Interestingly, the TIO basin continued to warm but at a slower rate of $0.011 \pm 0.004^{\circ}\text{Cyear}^{-1}$ during that hiatus period. The highest warming in the region is mainly located in the northwestern part on the centennial scale (Fig. 1j), and the warming has been expanded to equatorial and south TIO regions in recent decades (Fig. 1k&l). The basin averaged warming rate of TIO has been increased significantly during 1957-2017 ($0.013 \pm 0.001^{\circ}\text{Cyear}^{-1}$) as compared to 1900-1956 ($0.0037 \pm 0.0015^{\circ}\text{Cyear}^{-1}$) period with a mean surface temperature increment of $0.4 \pm 0.05^{\circ}\text{C}$ (Fig. S3). The warming has been amplified to 0.4°C ,

especially in the western tropical Indian Ocean and equatorial basin during the past six decades. The agreement among different SST products provides greater confidence to believe in the basin-wide warming trends.

The contribution from various modes of climate variations, particularly related to the TIO, needs to be adequately identified to understand the global ocean's anthropogenic surface warming properly. We performed the LFC analysis of the Tropical Indian Ocean SSTs to understand those variabilities. We adopted the first four leading modes to examine the variability pattern and its legible signature in the Indian Ocean. In our analysis, the global warming mode observed for TIO and global tropical oceans (Fig. 2a) is almost identical to that described by Wills et al. (2018) for the Pacific basin. The global warming pattern is nearly uniform for the period 1900-2017, without any typical signature of ENSO and IOD in the Pacific and Indian Oceans (Fig. S4). The LFC1 shows the warming trend of TIO, which is indistinguishable from global tropical oceans, especially in recent decades (Fig. 2b). During P1, the amplitude of the global warming signal peaks over the TIO, western Pacific, and the Atlantic Ocean. A very clear inter-basin contrast can be seen during P2 and P3, where the amplitude of warming weakens in the eastern Pacific (Fig. S4). The robust inter-basin warming contrast is the unique feature of TIO warming. The amplitude of warming weakens in the Pacific associated with the ongoing TIO warming trend. Using coupled model pacemaker experiments, Zhang et al. (2019) showed that warming in the Indian Ocean could effectively reduce the Pacific warming response to anthropogenic greenhouse gases. They further showed that enhanced trade winds driven by the zonal sea level pressure anomalies associated with the TIO warming, in turn, can reduce the SST in the eastern tropical Pacific by evaporative cooling and equatorial upwelling. In the TIO, the leading low-frequency spatial pattern indicates basin-wide warming (Basin mode, e.g., Chowdary and Gnanaseelan, 2007) with patches of enhanced warming north Indian Ocean during P1 and south tropical Indian Ocean during the periods P2 and P3 (Fig. S5). The LFC analysis gives a clear overview of the regional amplification of SST warming in the global tropical oceans.

Figure 2c displays a distinctive SST signature of warming centered in the Indian Ocean subtropical region (Mascarene high) region. The high-pressure area near the Mascarene Islands, the Indian Ocean subtropical high, undergoes substantial Interannual variability (Behera and Yamagata 2001). Using observation and reanalysis products, Vidya et al. 2020 reported that the SST anomalies under the Mascarene High region showed a higher variability and warming trend in recent decades. We extract SST anomalies over the area between 20°S-40°S and 45°E-100°E (Vidya et al., 2020) to relate LFC-2, and the time series are shown in Figure 2d. The LFP-2 accounts for 10% of low-

frequency SST variability of TIO, and corresponding LFC shows a statistically significant correlation of 0.5 with SST anomalies averaged of this region.

Interestingly, the third low-frequency mode of SST anomalies in the TIO denotes the subtropical Indian Ocean dipole (SIOD) mode (Behera and Yamagata 2001). The SIOD mode is characterized by negative (positive) SST anomalies occurring in the southeast Indian Ocean basin and positive (negative) SST anomalies occurring in the western basin southeast of Madagascar during its positive (negative) phase (Reason, 2001; Behera and Yamagata, 2001; Suzuki et al. 2004). The LFP-3 shows the negative phase of SIOD, and the LFC-3 is strongly negatively correlated (0.75) to the SIOD index, and this mode explains 8.3% of low-frequency SST variability (Fig. 2e,f). ENSO accounts for the fourth leading low-frequency mode in the TIO and contributes to 7.3% of SST variability (Fig. 2g,h). The distinct SST signatures of El Niño characterise warm SST anomalies extended from south-central to the north-western Indian Ocean. Apart from the anthropogenic global warming, the western and central Indian Ocean regions experience warming due to the El Niño. The disentangled modes of climate variabilities depict the spatial and temporal distinction of their signatures in SST anomalies.

3.2 Role of natural vs anthropogenic factors in long-term warming

Chen and Tung, (2018), based on a rotated EOF analysis, showed that Pacific and Atlantic Oceans contribute strongly to the global mean warming through ENSO at interannual scale and AMO at multi-decadal time scales respectively. They decomposed the global SST spatial patterns to global warming trend and climate modes. Using a signal-to-noise maximising EOF (LFC) analysis, we distinguished the warming trend of global tropical oceans and found that TIO, particularly equatorial regions, are in phase with warming elsewhere in the global tropics (Fig. S4). Hence, we analyse the roles of prominent global climate modes on TIO warming, which is an inevitable component of global mean surface temperature warming. Although the leading LFCs for global tropical oceans and TIO appear to be indistinguishable, especially in the recent decades (Fig. 2b). Hence, we consider the LFC-1 of TIO to quantify further the SST variability associated with anthropogenic warming. The LFC-1 amplitude remains same for the overlapping period whereas the location of peak warming has been significantly changed as seen in Fig. S5. Following Lean and Rind (2008) and Folland et al. (2018), we perform a multiple linear regression analysis to decompose SST anomalies into variability related to anthropogenic as well as natural climate modes in addition to residual (independent of predictors) variability.

In the present study, natural modes of climate variability include ENSO, ENSO Modoki, IOD, PDO and AMO, SIOD, and the variability of the Indian Ocean subtropical high to link the SST variability

of TIO. The ENSO Modoki is shown to have significant control on Indian Ocean warming at interannual to inter-decadal variabilities significantly since the 1970s and were relatively weak and short-lived before that time (Seow, 2018). The AMO induces warming over the Arabian Sea through a Gill-type Rossby wave response during its positive phase (Sun et al., 2019). The PDO has less contribution to global mean surface warming compared to AMO, because of its compensating cooling and warming cycles in the north Pacific (Chen and Tung, 2018). The spatial distribution of global warming and climate mode impacts on TIO's long-term warming remains the same in P1-P3. However, considerable variation in their magnitude has been observed, especially during P3, where climate mode predominance has been observed over the vast area of TIO (Fig. 3). Based on a multiple linear regression analysis, we find that global warming accounts for 65% of SST variability in the central-eastern equatorial region of the Indian Ocean. Interestingly, we observe a profound influence of natural climate modes over the southern tropical Indian Ocean. The role of climate modes on SST variability is marginal in the northwestern part of TIO during the period 1900-1979. The climate modes play a significant role in the southwestern Indian Ocean, where the internal SST variability plays a vital role in modifying ocean-atmosphere interactions (Jochum and Murtugudde, 2005).

The SST variability over the TIO is linearly related to climate modes of internal and external origin (Fig. 3). Multiple linear regression analysis of SSTs with climate modes showed that around 35% of SST variability in the western Indian Ocean is contributed by climate modes combinedly, and 50% of variability over the remaining parts of the north Indian Ocean is attributed to global warming in the recent decades (Figures 3e&f). The long-term warming of the north Indian Ocean, to a large extent, is accounted for by anthropogenic and natural modes of variability. In the southern tropical Indian Ocean, climate modes dominate over anthropogenic global warming. Spatial distributions of SST variability related to climate modes in the region south of Sumatra and east of Madagascar Islands feature IOD and SIOD in driving the variabilities over the south TIO region. The warming south of 10°S is mostly influenced by oceanic Rossby waves and Indonesian throughflow volume transport (Dong and McPhaden, 2016). The results presented in the study reveal the influences of various modes of climate variability on persistent warming of Indian Ocean overlaid with the high-frequency internal fluctuations. This has important implications given that the strength and phase of physical climate modes are sensitive to the monotonous warming of the northern Indian Ocean in a warming context.

3.3 Mechanisms of warming

3.3.1 Surface wind response to warming in the tropical Indian Ocean

The monotonous warming of the TIO has been accelerated in the past half-century. In this context, we shall try to understand the surface wind changes in the TIO during the past decades. Several studies have shown that the summer monsoon circulation in recent decades was weakened due to Indian Ocean warming (e.g., Kumar et al., 2009; Krishnan et al., 2013; Swapna et al., 2014). Together with anomalous westerly winds along the equator, the zonal wind speed component shows an increase of 0.035 ms^{-1} per year during the past half-century (Fig. 4a & 4b). The weakening of zonal winds north of 10°N and an anomalous weak anticyclonic circulation over the Indian landmass (Fig. 4c) suggest weakened monsoon surface flow. Kumar et al. (2009) reported that the equatorial westerlies under the warming over the TIO is associated with shear zone over the eastern TIO formed as a consequence of warming over the eastern Indian Ocean. The strengthening of equatorial westerlies leads to the significant increase of equatorial currents such as the Wyrki jet and increase of eastward heat transport (Gnanaseelan et al., 2017), which in turn warm the eastern equatorial Indian Ocean (Krishnan et al., 2006; Swapna et al., 2014).

Weakening of summer monsoon surface winds illustrated in previous studies (Swapna et al., 2014; Roxy et al., 2015) shown to have a predominant role in annual mean surface wind field trend shown in Figure 4b. Weakened cross-equatorial flow and associated north easterlies are observed over the Arabian Sea and Indian landmass and forming cyclonic surface circulation (Fig. 4b). Surface wind speed shows weakening trend of 0.02ms^{-1} in the north Indian Ocean except off the Oman coast and regions close to central equatorial Indian Ocean. Distribution of wind stress curl trend indicates positive curl over the Arabian Sea, which indicates strengthening of cyclonic circulation over Arabian Sea region (Fig. 4c). Over the western equatorial Indian Ocean, the anticyclonic wind stress curl and convergence of westerlies can suppress the equatorial upwelling and can enhance the warming there (Figs. 4b, 4c). The suppression of upwelling-related oceanic cooling has been argued to be one of the main causes of the recent surface warming trend in the equatorial Indian Ocean during the summer monsoon (Alory and Meyers, 2009). More frequent El Niño events in the recent decades have contributed to the warming of Indian Ocean and weakening of monsoon circulation (Roxy et al., 2014). Previous studies have also suggested that the weakened land-sea thermal contrast has played a key role in the weakening of surface winds over the Arabian Sea (Parvathi et al., 2017; Mohan et al., 2019).

The spatial patterns of wind speed and wind vectors depicted in Figure 4d are obtained by correlating Indian Ocean warming signal on wind speed and regressing zonal and meridional wind

speed components. It is noticed that the equatorial westerlies originated in the western Indian Ocean are dominant in response to the Indian Ocean warming. It is also interesting to note that the trend in the form of a low-level cyclonic flow in the Arabian Sea (shown in Figure 4b) is directly related to the warming of the TIO. The northeasterly winds over the southern Indian landmass and the Arabian Sea are seen to converge toward the equatorial Indian Ocean and lead to enhanced equatorial westerly anomalies as a consequence of the TIO warming trend (Figs. 4b & 4d). The weakened climatological easterlies south of the equator during the summer monsoon season have favored strengthening of westerlies. The features remain the same for 1980-2017, and strong winds eastward in the equatorial Indian Ocean is also observed (Fig. S6). In short, the surface winds have a cyclonic circulation trend over the Arabian Sea region and northeasterlies and southwesterlies converge to the equatorial Indian Ocean, which in turn acts to intensify the wind speed over the central equatorial Indian Ocean.

3.3.2 Role of surface heat fluxes

Many previous studies have reported the monotonous warming of the Indian Ocean since the last five decades (e.g., Levitus et al., 2000; Alory et al., 2007; Rao et al., 2012) and it is believed to be due to global net surface heat flux changes. In this context, we examine the trends in surface air-sea fluxes, out-going longwave radiation (OLR) at the top of the atmosphere and total cloud cover and shown in Figure 5. The net heat flux into the ocean is the sum of heat gain due to shortwave radiation (Q_{sw}) and heat loss due to longwave radiation (Q_{lw}), sensible heat flux (Q_{shf}), and latent heat flux (Q_{lhf}). It is important to explore the relative role of each component behind the basin-wide warming of TIO. In this paper, positive value denotes the flux upward of ocean. The Q_{sw} shows a positive trend over the western and southern parts of the basin associated with an increase in the tendency of total cloud cover (Figs. 5a & 5g). In phase with the reduction of cloud cover, the net shortwave flux shows an increase in trend over land and southern subtropical Indian Ocean. The surface shortwave radiation trend follows the cloudiness over the northern Indian Ocean. The trend in net surface longwave radiation depends on the downward longwave radiation due to greenhouse gases and water vapour concentrations. As expected in a warming context, the net longwave flux shows a negative trend due to the increase in downward longwave flux. Based on observation records, Wild et al. (2017) reported that the downward longwave radiation had shown an increase of $2 \text{ Wm}^{-2}\text{decade}^{-1}$ since the 1990s in line with the increase in greenhouse effects. The positive contributions of surface net longwave radiation and latent heat from the atmosphere are due to increased greenhouse gases in the atmosphere (Dong et al., 2014). Increase in cloud cover traps more upward longwave radiations and radiate it back to the surface and can enhance surface warming (Figs. 5g & 6g).

Spatial distribution of linear trend pattern for the period 1948-2017 shows that the loss of latent heat out of the ocean has been increased over the central equatorial Indian Ocean, the south-eastern Indian Ocean and the north-western Indian Ocean. Contrasting Q_{lhf} variations can be seen in the southeastern Arabian Sea and southwestern Bay of Bengal adjacent to southern peninsular India. The positive contributions of surface net longwave radiation are compensated by an increase in Q_{lhf} and Q_{shf} out of the ocean (Fig. 5c). Based on the analysis of heat flux products, Rahul and Gnanaseelan (2013) concluded that the net heat flux over the central TIO has a decreasing trend due to the increase of Q_{lhf} associated with increased SST and wind speed. The decrease in net heat flux results from the loss of latent heat out of the ocean except over the eastern Arabian Sea and the southwestern Bay of Bengal. It is noteworthy that the SST warming is more profound over the regions in spite of the large Q_{lhf} release and this signifies the role of ocean dynamics in driving monotonous warming of TIO. In the north Indian Ocean, the Q_{lhf} variability is largely controlled by the thermodynamic processes during the summer monsoon period (Kumar et al., 2017). The strong positive trend in Q_{lhf} in the central equatorial Indian Ocean is probably due to stronger westerlies associated with the weakening of southwest monsoon (Fig. 4). Figures 4b and 5c show that the Q_{lhf} trend is largely in phase with the changes in wind speed as suggested by Dong et al. (2014). The net heat flux gain into the ocean in the Bay of Bengal and the eastern Arabian Sea, particularly along the coastlines, is attributed to the reduced Q_{lhf} caused by the weakened wind speed.

The Indian Ocean warming signal (shown in Fig. 2b) is linearly related to the trends of surface air-sea fluxes (Fig. 6). The spatial correlation pattern is statistically significant at 95% confidence level. However, the net flux distribution tends to cool most of the tropical Indian Ocean. The increase in wind speed in the equatorial region cause Q_{lhf} increase in a warming scenario and leads to negative net flux trend (Tomita and Kubota, 2010). Alory and Meyers (2009) suggest that the ocean dynamics plays a major role in the SST warming of equatorial Indian Ocean. Previous researches revealed the decreasing trend of Q_{net} in the tropical Indian Ocean and suggested that the imbalance of air-sea fluxes plays a secondary role relative to ocean dynamics in warming of TIO (e.g., Chowdary and Gnanaseelan, 2007; Rahul and Gnanaseelan, 2013).

Spatial distribution of trends in the OLR, a proxy for tropical convection indicates a reduction in the central to eastern equatorial Indian Ocean and increment elsewhere in the northern Indian Ocean. The basin-wide warming of Indian Ocean eventually leads to latent heat loss from the ocean due to the reduction of OLR and which in turn enhance the premonsoon rainfall trend over the Bay of Bengal (Chaudhari et al., 2018). The reduction of OLR in recent decades is attributed to longwave absorption

by higher greenhouse gas levels (Dong et al., 2014). In CMIP5 climate models, the OLR reduction associated with the greenhouse gas forcing is alleviated within few decades, and global warming is caused by enhanced net absorption of solar radiation (Donohoe et al., 2014). In Figure 6f, a significant negative correlation in OLR with Indian Ocean warming signal can be observed in the eastern and equatorial regions of the Indian Ocean, which signified enhanced warming and convection over there. The positive correlation of OLR can be seen over the landmasses, the southwestern Indian Ocean, south-eastern the Arabian Sea adjacent to the Western Ghats and Bay of Bengal. Consequently, the spatial distribution of OLR trend indicates a decrease in convective activities over these regions (Fig. 5f). The changes in OLR, surface heat fluxes and equatorial westerly winds indicate that the convection over the central equatorial Indian Ocean has been enhanced in a warming context. We also examine the trends in heat flux components for the period 1980-2017 and considerable change in spatial distribution is observed relative to the past century variations (Fig. S7 and S8). Surface net shortwave gain due to the reduction of cloud cover over the central Indian Ocean region has been observed and lead to Q_{lhf} loss and decline in Q_{net} also observed.

The mechanisms for the basin-wide warming are further illustrated by examining the mixed layer heat content and heat budget and described in the following sections.

3.3.3. Mixed layer heat budget

3.3.3.1 Heat content of the mixed layer

The heat content of the water column within the mixed layer of the ocean is crucial in view of air-sea interaction in a warming context. The estimate of upper ocean heat content trend would facilitate to explain how the mixed layer heat budget of the tropical Indian Ocean is adjusting in a warming context. Spatial trend distribution of mixed layer heat content increases over the eastern equatorial Indian Ocean, the Bay of Bengal, and the south Indian Ocean, with magnitudes ranging from 0.5 to $3 \times 10^7 \text{ Jm}^{-2}\text{year}^{-1}$ during the past three decades (Fig. 7a). The peak warming locations are shown in Figure 8a also fall in these regions of accelerated heat content trend. Contrary to the basinwide warming trends, the heat content trends are negative over most of the Arabian Sea, western equatorial Indian Ocean and regions close to the equator with the largest magnitudes of about $-2 \times 10^7 \text{ Jm}^{-2}\text{year}^{-1}$. This signifies the role of ocean dynamics on the basin-wide warming of TIO region. Excess heat uptake of eastern equatorial Indian Ocean can be attributed to the eastward heat transport of equatorial currents driven by strengthened westerly winds over the equatorial Indian Ocean as suggested by Gnanaseelan et al. (2017). The positive trend in mixed layer heat content of the south Indian Ocean indicates the

role of heat transport from Pacific into the south Indian Ocean through the Indonesian passages (cf. Lee et al. 2015).

A thick mixed layer has a larger heat capacity and hence modulates the intensity of SST warming. The regions of increase in heat content (Fig. 7a) are regions where MLD is deep in response to TIO warming (Fig. 7c). Based on the analysis of coupled general circulation models, Yeh et al. (2009) showed that deeper (shallower) the simulated MLD, the lesser (higher) the warming rate. But, the present study shows that mixed layer temperature trend increases with increase in heat content in the south tropical regions (Fig. 8a and Fig. 7a). We also examined the mixed layer stratification, which can be inferred from the density gradient between the surface and subsurface layers of the mixed layer, represented by the static stability parameter (Pond and Pickard 1983). The static stability of mixed layer exhibits increasing trend over the western Arabian Sea and regions close to western to central equatorial Indian Ocean during the recent decades (Fig. 7b). The MLD has been shoaled significantly over the regions of a significant increase in static stability (Fig. S9b), particularly over the Arabian Sea, where the mixed layer is deep climatologically (Fig. S9a). The decline of static stability, in line with the strengthened winds (Fig. S6) over the equatorial Indian Ocean, has contributed to an anomalously deep mixed layer over there leading to an increase in heat content.

Enhanced mixed layer stratification and shoaling of mixed layer in turn can accelerate the warming of north Indian Ocean as compared to the southern regions. The MLD in the western Indian Ocean and the Arabian Sea regions are attributed to the surface stratification associated with weakening of the upwelling favorable winds. Kumar and Narvekar (2005) have shown that the MLD of Arabian Sea basin to a large extent is controlled by the wind forcing. The cyclonic circulation and positive wind stress curl trends in the Arabian Sea, as shown in Figures S6(b&c) would have caused thin and stratified mixed layer. The spatial distribution of correlation coefficient between MLD and TIO warming signal for their common period (1980-2017) is shown in Figure 7c and which depicts that the MLD is deepened (shoaled) in the regions of decreased (increased) in static stability. The weakening of surface winds and cyclonic wind stress curl over the northern Indian Ocean basin leads to reduced mixing and hence shallow mixed layer, which in turn can cause the warming during the period of 1980-2017 (Fig. 1l) over a stratified thinner surface layer in the north Indian Ocean. The deep mixed layer owing to the strengthened equatorial winds would have reduced warming intensity of eastern equatorial Indian Ocean as seen in the SST trend derived from HadISST, ERSST, and ensemble mean (Figures 1c, f&l).

3.3.3.2 Mixed layer heat budget

The mixed layer heat budget estimation in the present study diagnoses the mixed layer temperature fluctuations due to atmospheric heat fluxes and oceanic processes for the period 1980-2017. The temperature averaged over the mixed layer is the same as the SST warming except for a few regions of localized cooling (Fig. 8a). We show the time-integrated heat budget components to examine the temperature change contributed by each component over the period considered. The net atmospheric heat flux contribution has significantly decreased by about 1°C, especially over the southern part of the tropical Indian Ocean. The positive contribution can be seen in the eastern equatorial region, where the temperature trend is relatively weak. The ocean's Q_{net} loss has significantly increased in equatorial and southeastern regions, where the surface net shortwave into the ocean has also been reduced (Fig. S7). In contrast, the Q_{lhf} and Q_{shf} loss out of the ocean (Figs. S7 c&d) signifies role of oceanic processes in warming the surface ocean.

To distinguish the roles played by horizontal advection processes, we have computed the temperature change due to zonal and meridional advection processes and shown in Figures 8c&d. The meridional advection has contributed to about 1°C rise in temperature in the south TIO, where the zonal advection has caused a marginal temperature rise of 0.2°C. The advection of heat transported from the south and eastern equatorial Indian Ocean to western equatorial Indian Ocean, which in turn transported zonally eastward, played a significant role in the basin-wide warming of the Indian Ocean in the recent decades. A remarkable agreement is noted between the diagnosed meridional advection component on the heat storage of the regions where the atmospheric contribution is negligible (Fig. 8b&d). The net surface heat flux gain of the Pacific Ocean has been increased significantly in the past decades (England et al., 2014), leading to an increase in subsurface ocean heat uptake (Meehl et al., 2011, 2013). Enhanced warm water transport from Western Pacific to the south Indian Ocean via Indonesian throughflow has been increased due to increased water volume in the Western Pacific and the accelerated Pacific trade winds (Wu et al., 2012). The spatial distribution of warming-related to horizontal advection has been observed from the south of the Indonesian Archipelago to the western equatorial Indian Ocean. Figure 8d shows that the slope of maximum temperature change is from the region southeast to northwest in the southern TIO, which suggests that the heat transport is related to the advection process by downwelling Rossby waves.

The subsurface vertical processes term in the heat budget represents the heating/cooling rate due to vertical advection ($\frac{-w_h}{h} (T_a - T_{-h})$) and entrainment mixing processes ($\frac{-1}{h} \frac{\partial h}{\partial t} (T_a - T_{-h})$) occurring at the mixed layer base. A decrease in wind stress curl in the south (Fig. S6c),

particularly strong in the southeast and westward of Australia is observed. This generates westward-propagating downwelling Rossby waves (Xie et al. 2002), which affect the mixed layer temperature and reduce the advective cooling. Previous studies reported that the Rossby waves from the south Indian Ocean appear to modulate the SST changes in TIO (Rao and Sivakumar, 2000, and references therein). The cooling induced by vertical processes found to be marginal, whereas it contributed to the warming rate of about 0.1°C during the period considered. As a consequence of these vertical advection processes and the westward horizontal advection process in the equatorial and southern Indian Ocean, the mixed layer remains thin, and stratification increases, which may have favoured persistent TIO warming. The advection processes are also profound in the north Indian Ocean. Advection of warm waters can be transported to high latitudes along the west coast of India. The vertical excursions of thermocline by downwelling process and planetary waves could be important in the redistribution of heat in the northern Indian Ocean.

The prominent feature of the long-term warming in TIO is that the oceanic processes reinforce the warming tendency, which counters the cooling by the net loss of surface heat flux. Statistically significant correlation coefficients between mixed layer temperature tendency and the sum of heat budget terms, including net heat flux, advection, and vertical processes, indicate a near closure of heat budget except for few localized regions of TIO (Fig. S10a). A full closure of the mixed layer heat budget is not feasible due to the uncertainties in surface heat fluxes, mixed layer thermal structure, and currents used for computation of heat budget terms. The uncertainties in mixed layer heat budget terms and unresolved processes contributes to the residual error. The relatively weaker magnitude of the temperature change due to residual term indicates the marginal role of unresolved processes, including lateral mixing and diffusion processes. The oceanic contribution changes to warming tendency are mostly due to enhanced meridional advection and a decrease in vertical advection and entrainment processes, which are the primary cooling terms of the heat budget formulated in the present study.

3.4 Long-term warming in Community Earth System Model version 2 (CESM2)

The mechanisms of the long-term warming of TIO is further examined using a climate model participating in Phase 6 of the Coupled Model Intercomparison Project (CMIP6). The Community Earth System Model version 2 (CESM2), a fully coupled state-of-the-art climate system model, is the upgraded version of CESM1, which was widely used for climate change studies across the globe (e.g., Larson et al., 2017; Wang et al., 2018). The CESM1 is reported to be one of the best models in the CMIP5 framework to simulate regional climate (Kamworapan et al., 2017; Zazulie et al., 2017). We examine the mechanisms of long-term warming in the CESM2 historical experiment for the period 1900-2014. The CESM2 reproduces the general warming trend of TIO, and the warming rate is

relatively large along the southeastern region (Fig. 9a). The CMIP5 climate models project a positive IOD like pattern and robust SST warming in the western equatorial Indian Ocean (Liu et al., 2015; Luo et al., 2016). However, few studies reported intermodel uncertainty of CMIP5 models in representing SST (e.g., Alory and Meyers, 2009; Zheng et al., 2016). Historical simulation of CESM2 shows basin wide warming but spatially non-uniform, with highest warming trends seen in the southeastern Indian Ocean and lowest trends in the southwestern part (Fig. 9a). In CESM2, long-term warming (1900-2014) is estimated to be 1°C over the 115-yr period. Though the model results are sometimes different from the observations, this model simulation provided us with an opportunity to study the oceanic and atmospheric co-variability in a coupled state, albeit virtually, for a long time period in the absence of quality observational data. For example, we examined the mixed layer heat budget analysis to explore the causes of warming as the temperature averaged in the mixed layer has the same long-term trend of SST.

The mechanism of long-term warming in CESM2 is straightforward and is directly linked to winds and net heat flux. The basin-wide shoaling of the mixed layer coincides with the declined winds in the CESM2 historical simulation. The moderately strengthened wind speed is observed westward along the equatorial region, and an eastward patch off Madagascar Island and corresponding MLD trend also can be seen in Figure 9c. The basin-wide weakening of surface wind is the leading cause of the warming pattern in CESM2. Figure S11 reveals that the net heat flux gain in the basin, unlike in the reanalysis, is due to the basin wide weakening of surface winds. The Q_{net} loss due to Q_{lhf} (latent heat flux) is restricted to the regions of the weak positive trend in surface winds, leading to a reasonable net heat gain into the ocean in CESM2. The weakened surface winds in the southeastern equatorial Indian Ocean inhibited the heat loss out of the ocean there, which forced the highest long-term warming over there in CESM2 historical simulation.

The sum of heat budget components reproduces the overall pattern of mixed layer temperature tendency term in CESM2 as shown by the spatial correlation map (Fig. S10b). The temperature tendency due to advection and vertical processes is significantly correlated with the heat storage rate. The largest positive correlation is seen over the southeastern Indian Ocean, signifying the role of Pacific volume transport to the Indian Ocean through the Indonesian throughflow system in CESM2 as in NCEP GODAS for 1980-2017. In the north Indian Ocean, horizontal advection and vertical processes act along with Q_{net} to favor the warming. The vertical processes, the main cooling term of mixed layer heat budget, have warmed the mixed layer at a rate of 0.2°C/115yr in few regions. The cooling is marginal except for the region westward off Sumatra (Fig. 9f). The significantly high correlation of temperature tendency with horizontal advection (Fig. 9d) and vertical processes (Fig.

9e) show their role in the long-term warming simulated by CESM2 historical simulation. The change of mixed layer temperature near the equatorial regions, particularly southern subtropics, western and central regions, are related to oceanic advection and vertical processes besides the weakening of the surface wind there.

4. Summary and Conclusions

Previous studies suggest SSTs over the tropical Indian Ocean region show interannual, decadal, and multi-decadal variations superimposed on a robust warming trend. However, the quantification and the causes of the long-term SST variability remain unclear. Here, we investigate the SST variability at a long-term scale in the TIO by analysing ensemble mean SST anomalies constructed from three gridded reanalysis products for 118 years (1900-2017) and a CMIP6 climate model historical simulation for 115 years (1900-2014). The highest warming in the region is mainly located in the northwestern part at the centennial scale, and the warming has been expanded to equatorial and south TIO regions in recent decades. The basin averaged warming rate of TIO has been increased significantly during 1957-2017 ($0.013 \pm 0.001^{\circ}\text{Cyear}^{-1}$) with reference to 1900-1956 ($0.0037 \pm 0.0015^{\circ}\text{Cyear}^{-1}$) period with a mean surface temperature increment of $0.4 \pm 0.05^{\circ}\text{C}$. The warming has been amplified to 0.4°C , especially in the western tropical Indian Ocean and equatorial basin during the past six decades. The consensus of different SST products provides greater confidence to believe in the basin wide warming trends. The long-term warming of the TIO is synchronized with the leading mode of SST variability of global tropical oceans and is in phase with the warming of tropical western Pacific and Atlantic Oceans. The warming trends of the western and eastern equatorial Indian Ocean, to a great extent, are accounted by natural modes of climate variability.

In response to the warming of TIO, surface winds show a weakening trend over a large area of the north Indian Ocean, and anomalous westerlies are observed along the equator. The weakening of cross-equatorial flow, along with the northeasterly winds from the Arabian Sea, has accelerated the cyclonic circulation of the basin, and that strengthens the westerly surface winds along the equator. Anticyclonic wind stress curl and convergence of westerlies suppress the equatorial upwelling and cause anomalous warming of the western equatorial Indian Ocean. Over the TIO, the heat flux trend is dominated by offsetting anomalies of radiative fluxes and latent heat flux. The decrease in cloud cover forces an increase of flux into the ocean and is countered by excess loss of latent heat out of the ocean as a consequence of strengthened equatorial westerlies. The convergence of northeasterly winds over the equatorial region drives the heat loss from the ocean, which overcomes the radiative warming. The thermodynamical forcing discussed in the present study had operated in the forcing mechanism of extreme positive IOD event occurred in 2019 (Wang et al., 2020). Their study also suggests that the

ongoing TIO warming trend has possible ramifications on IOD through this unique thermodynamical forcing. Coupled model experiments project a robust SST warming in the western equatorial Indian Ocean due to the occurrence of frequent positive IOD in the Indian Ocean (Luo et al., 2016).

The mixed layer has been shoaled in the Arabian Sea and western equatorial Indian Ocean in recent decades, which leads to an increase in stratification there. Surface circulation changes associated with the cyclonic circulation and positive wind stress curl trend have triggered shoaling of the mixed layer, which in turn caused the warming of stratified surface layers in the north Indian Ocean. The meridional advection has contributed to about 1°C rise in temperature in the south TIO, where the zonal advection has caused a marginal temperature rise of 0.2°C. The oceanic cooling by vertical processes, including entrainment and vertical advection, has been suppressed in the TIO. The advection of heat transported from the southeastern equatorial Indian Ocean to the western equatorial Indian Ocean, which in turn transported zonally eastward, played a significant role in the basin-wide warming of the Indian Ocean in the recent decades. The prominent feature of the long-term warming of the TIO is the oceanic processes reinforce the warming tendency, which counters the cooling by the net loss of surface heat flux.

The mechanism of long-term warming in CESM2 is linked to basin wide weakening of surface winds associated net heat flux gain into the ocean. Heat transport by horizontal advection and suppressed oceanic cooling by vertical processes also favoured the basin wide warming in CESM2 historical simulation. Progress to better projections of global mean surface warming depends on our understanding of the multiple causes of climate trends and its variations. Present work quantifies the long-term warming of the tropical Indian Ocean, which is in phase with the global mean surface warming. Rigorous scale analysis of SST variabilities and possible mechanisms described in the present study would help to understand the multiple causes of the long-term warming of the Indian Ocean.

Acknowledgements

This research is partly supported by the DST Centre of Excellence in Climate Modeling. The authors thank all the modeling and research centres for making the data available i.e. HadISST, ERSST, COBE, NCEP and GODAS. We thank <https://esgfnode.llnl.gov/> and <http://archive.ceda.ac.uk/> for making available the CESM2 historical simulations. This is NIO contribution no. xxxx.

References

- Alory, G. and Meyers, G., 2009. Warming of the upper equatorial Indian Ocean and changes in the heat budget (1960–99). *Journal of Climate*, 22(1), 93-113.
- Alory, G., Wijffels, S. and Meyers, G., 2007. Observed temperature trends in the Indian Ocean over 1960–1999 and associated mechanisms. *Geophysical Research Letters*, 34(2).
- Ashok, K., Behera, S.K., Rao, S.A., Weng, H. and Yamagata, T., 2007. El Niño Modoki and its possible teleconnection. *Journal of Geophysical Research: Oceans*, 112(C11).
- Ashok, K. and Yamagata, T., 2009. The El Niño with a difference. *Nature*, 461(7263), 481-484.
- Behera, S. and Yamagata, T., 2010. Imprint of the El Niño Modoki on decadal sea level changes. *Geophysical Research Letters*, 37(23).
- Behera, S.K. and Yamagata, T., 2001. Subtropical SST dipole events in the southern Indian Ocean. *Geophysical Research Letters*, 28(2), 327-330.
- Behringer, D. and Xue, Y., 2004. Evaluation of the global ocean data assimilation system at NCEP: The Pacific Ocean, Proc. Eighth Symp. on Integrated Observing and Assimilation Systems for Atmosphere, Oceans, and Land Surface. AMS 84th Annual Meeting, Washington State Convention and Trade Center
- Bhowmick, M., Sahany, S. and Mishra, S.K., 2019. Projected precipitation changes over the south Asian region for every 0.5 C increase in global warming. *Environmental Research Letters*, 14(5), 054005.
- Cai, W. et al., 2007. Anthropogenic aerosol forcing and the structure of temperature trends in the southern Indian Ocean. *Geophysical Research Letters*, 34(14).
- Chaudhari, H.S. et al., 2018. SST and OLR relationship during Indian summer monsoon: a coupled climate modelling perspective. *Meteorology and Atmospheric Physics*, 130(2), 211-225.
- Chen, M., Yu, J.Y., Wang, X. and Jiang, W., 2019. The changing impact mechanisms of a diverse El Niño on the western Pacific subtropical high. *Geophysical Research Letters*, 46(2), 953-962.
- Chen, X. and Tung, K.-K., 2018. Global surface warming enhanced by weak Atlantic overturning circulation. *Nature*, 559(7714), 387-391.
- Chowdary, J. and Gnanaseelan, C., 2007. Basin-wide warming of the Indian Ocean during El Niño and Indian Ocean dipole years. *International Journal of Climatology: A Journal of the Royal Meteorological Society*, 27(11), 1421-1438.
- Deser, C., Alexander, M.A., Xie, S.-P. and Phillips, A.S., 2010. Sea surface temperature variability: Patterns and mechanisms. *Annual review of marine science*, 2, 115-143.
- Dong, L. and McPhaden, M.J., 2016. Interhemispheric SST gradient trends in the Indian Ocean prior to and during the recent global warming hiatus. *Journal of Climate*, 29(24), 9077-9095.

- Dong, L. and Zhou, T., 2014. The Indian Ocean sea surface temperature warming simulated by CMIP5 models during the twentieth century: Competing forcing roles of GHGs and anthropogenic aerosols. *Journal of Climate*, 27(9), 3348-3362.
- Donohoe, A., Armour, K.C., Pendergrass, A.G. and Battisti, D.S., 2014. Shortwave and longwave radiative contributions to global warming under increasing CO₂. *Proceedings of the National Academy of Sciences*, 111(47), 16700-16705.
- Douville, H. et al., 2000. Impact of CO₂ doubling on the Asian summer monsoon. *Journal of the Meteorological Society of Japan. Ser. II*, 78(4), 421-439.
- Enfield, D.B., Mestas-Nuñez, A.M. and Trimble, P.J., 2001. The Atlantic multidecadal oscillation and its relation to rainfall and river flows in the continental US. *Geophysical Research Letters*, 28(10), 2077-2080.
- England, M.H. et al., 2014. Recent intensification of wind-driven circulation in the Pacific and the ongoing warming hiatus. *Nature climate change*, 4(3), 222-227.
- Exarchou, E., Prodhomme, C., Brodeau, L., Guemas, V. and Doblas-Reyes, F., 2018. Origin of the warm eastern tropical Atlantic SST bias in a climate model. *Climate Dynamics*, 51(5-6), 1819-1840.
- Eyring, V. et al., 2016. Overview of the Coupled Model Intercomparison Project Phase 6 (CMIP6) experimental design and organization. *Geoscientific Model Development*, 9(5), 1937-1958.
- Folland, C.K., Boucher, O., Colman, A. and Parker, D.E., 2018. Causes of irregularities in trends of global mean surface temperature since the late 19th century. *Science advances*, 4(6), eaao5297.
- Girishkumar, M. S., Ravichandran, M., & McPhaden, M. J. (2013). Temperature inversions and their influence on the mixed layer heat budget during the winters of 2006–2007 and 2007–2008 in the Bay of Bengal. *Journal of Geophysical Research: Oceans*, 118(5), 2426-2437.
- Gnanaseelan, C., Roxy, M. and Deshpande, A., 2017. Variability and trends of sea surface temperature and circulation in the Indian Ocean, Observed climate variability and change over the Indian Region. Springer, pp. 165-179.
- Han, W. et al., 2014. Indian Ocean decadal variability: A review. *Bulletin of the American Meteorological Society*, 95(11), 1679-1703.
- Hirahara, S., Ishii, M. and Fukuda, Y., 2014. Centennial-scale sea surface temperature analysis and its uncertainty. *Journal of Climate*, 27(1), 57-75.
- Hurrell, J.W. et al., 2013. The community earth system model: a framework for collaborative research. *Bulletin of the American Meteorological Society*, 94(9), 1339-1360.
- Ishii, M., Shouji, A., Sugimoto, S. and Matsumoto, T., 2005. Objective analyses of sea-surface temperature and marine meteorological variables for the 20th century using ICOADS and the Kobe collection. *International Journal of Climatology: A Journal of the Royal Meteorological Society*, 25(7), 865-879.

- Jochum, M. and Murtugudde, R., 2005. Internal variability of Indian ocean SST. *Journal of climate*, 18(18), 3726-3738.
- Kalnay, E. et al., 1996. The NCEP/NCAR 40-year reanalysis project. *Bulletin of the American meteorological Society*, 77(3), 437-472.
- Kamworapan, S. and Surussavadee, C., 2017. Performance of cmip5 global climate models for climate simulation in southeast Asia, TENCON 2017-2017 IEEE Region 10 Conference. IEEE, pp. 718-722.
- Kistler, R. et al., 2001. The NCEP–NCAR 50-year reanalysis: monthly means CD-ROM and documentation. *Bulletin of the American Meteorological society*, 82(2), 247-268.
- Kosaka, Y. and Xie, S.-P., 2013. Recent global-warming hiatus tied to equatorial Pacific surface cooling. *Nature*, 501(7467), 403-407.
- Krishnan, R. et al., 2006. Indian Ocean-monsoon coupled interactions and impending monsoon droughts. *Geophysical research letters*, 33(8).
- Krishnan, R. et al., 2013. Will the South Asian monsoon overturning circulation stabilize any further? *Climate dynamics*, 40(1-2), 187-211.
- Kucharski, F. and Abid, M.A., 2017. Interannual variability of the Indian monsoon and its link to ENSO, *Oxford Research Encyclopedia of Climate Science*.
- Kucharski, F., Syed, F., Burhan, A., Farah, I. and Gohar, A., 2015. Tropical Atlantic influence on Pacific variability and mean state in the twentieth century in observations and CMIP5. *Climate Dynamics*, 44(3), 881-896.
- Kug, J.-S., Jin, F.-F. and An, S.-I., 2009. Two types of El Niño events: cold tongue El Niño and warm pool El Niño. *Journal of Climate*, 22(6), 1499-1515.
- Kumar, B.P., Cronin, M.F., Joseph, S., Ravichandran, M. and Sureshkumar, N., 2017. Latent heat flux sensitivity to sea surface temperature: Regional perspectives. *Journal of Climate*, 30(1), 129-143.
- Kumar, M.R., Krishnan, R., Sankar, S., Unnikrishnan, A. and Pai, D., 2009. Increasing trend of “break-monsoon” conditions over India—role of ocean–atmosphere processes in the Indian Ocean. *IEEE Geoscience and Remote Sensing Letters*, 6(2), 332-336.
- Kumar, S.P. and Narvekar, J., 2005. Seasonal variability of the mixed layer in the central Arabian Sea and its implication on nutrients and primary productivity. *Deep Sea Research Part II: Topical Studies in Oceanography*, 52(14-15), 1848-1861.
- Larson, S.M., Kirtman, B.P. and Vimont, D.J., 2017. A framework to decompose wind-driven biases in climate models applied to CCSM/CESM in the eastern Pacific. *Journal of Climate*, 30(21), 8763-8782.
- Lean, J.L. and Rind, D.H., 2008. How natural and anthropogenic influences alter global and regional surface temperatures: 1889 to 2006. *Geophysical Research Letters*, 35(18).

- Lee, S.-K. et al., 2015. Pacific origin of the abrupt increase in Indian Ocean heat content during the warming hiatus. *Nature Geoscience*, 8(6), 445-449.
- Levitus, S., Antonov, J.I., Boyer, T.P. and Stephens, C., 2000. Warming of the world ocean. *Science*, 287(5461), 2225-2229.
- Li, Y., W. Han, and L. Zhang (2017), Enhanced decadal warming of the southeast Indian Ocean during the recent global surface warming slowdown, *Geophysical Research Letters*, 44(19), 9876-9884.
- Li, X., Xie, S.-P., Gille, S.T. and Yoo, C., 2016. Atlantic-induced pan-tropical climate change over the past three decades. *Nature Climate Change*, 6(3), 275-279.
- Liu, W., Lu, J. and Xie, S.-P., 2015. Understanding the Indian Ocean response to double CO₂ forcing in a coupled model. *Ocean Dynamics*, 65(7), 1037-1046.
- Liu, W. and Xie, S.-P., 2018. An ocean view of the global surface warming hiatus. *Oceanography*, 31(2), 72-79.
- Lukas, R. and Lindstrom, E., 1991. The mixed layer of the western equatorial Pacific Ocean. *Journal of Geophysical Research: Oceans*, 96(S01), 3343-3357.
- Luo, J.-J., Sasaki, W. and Masumoto, Y., 2012. Indian Ocean warming modulates Pacific climate change. *Proceedings of the National Academy of Sciences*, 109(46), 18701-18706.
- Luo, Y., Lu, J., Liu, F. and Wan, X., 2016. The positive Indian Ocean Dipole-like response in the tropical Indian Ocean to global warming. *Advances in Atmospheric Sciences*, 33(4), 476-488.
- Mantua, N.J., Hare, S.R., Zhang, Y., Wallace, J.M. and Francis, R.C., 1997. A Pacific interdecadal climate oscillation with impacts on salmon production. *Bulletin of the American Meteorological Society*, 78(6), 1069-1080.
- McPhaden, M. J., & Hayes, S. P. (1991). On the variability of winds, sea surface temperature, and surface layer heat content in the western equatorial Pacific. *Journal of Geophysical Research: Oceans*, 96(S01), 3331-3342.
- Meehl, G.A., Arblaster, J.M., Fasullo, J.T., Hu, A. and Trenberth, K.E., 2011. Model-based evidence of deep-ocean heat uptake during surface-temperature hiatus periods. *Nature Climate Change*, 1(7), 360-364.
- Meehl, G.A., Hu, A., Arblaster, J.M., Fasullo, J. and Trenberth, K.E., 2013. Externally forced and internally generated decadal climate variability associated with the Interdecadal Pacific Oscillation. *Journal of Climate*, 26(18), 7298-7310.
- Mishra, S.K., Jain, S., Salunke, P. and Sahany, S., 2019. Past and future climate change over the Himalaya-Tibetan Highland: inferences from APHRODITE and NEX-GDDP data. *Climatic Change*, 156(3), 315-322.
- Mohan, S. and Bhaskaran, P.K., 2019. Evaluation of CMIP5 climate model projections for surface wind speed over the Indian Ocean region. *Climate Dynamics*, 53(9-10), 5415-5435.

- Narvekar, J. and Kumar, S.P., 2014. Mixed layer variability and chlorophyll a biomass in the Bay of Bengal. *Biogeosciences*, 11, 3819–3843.
- Nishida, T., Kitakado, T. and Matsuura, H., 2011. Validation of the Global Ocean Data Assimilation System (GODAS) data in the NOAA National Centre for Environmental System (NCEP) by theory, comparative studies, applications and sea truth. Victoria, Seychelles.
- Pond, S. and Pickard, G., 1983. *Introductory dynamical oceanography*. Butterworth Heinemann. Oxford.
- Parvathi, V., Suresh, I., Lengaigne, M., Izumo, T. and Vialard, J., 2017. Robust projected weakening of winter monsoon winds over the Arabian Sea under climate change. *Geophysical Research Letters*, 44(19), 9833-9843.
- Rahul, S. and Gnanaseelan, C., 2012. Net heat flux over the Indian Ocean: trends, driving mechanisms, and uncertainties. *IEEE Geoscience and Remote Sensing Letters*, 10(4), 776-780.
- Rao, R. and Sivakumar, R., 2000. Seasonal variability of near-surface thermal structure and heat budget of the mixed layer of the tropical Indian Ocean from a new global ocean temperature climatology. *Journal of Geophysical Research: Oceans*, 105(C1), 995-1015.
- Rao, S.A. et al., 2012. Why is Indian Ocean warming consistently? *Climatic change*, 110(3-4), 709-719.
- Rasmusson, E.M. and Carpenter, T.H., 1982. Variations in tropical sea surface temperature and surface wind fields associated with the Southern Oscillation/El Niño. *Monthly Weather Review*, 110(5), 354-384.
- Rayner, N. et al., 2003. Global analyses of sea surface temperature, sea ice, and night marine air temperature since the late nineteenth century. *Journal of Geophysical Research: Atmospheres*, 108(D14).
- Rayner, N.A. et al., 2006. Improved analyses of changes and uncertainties in sea surface temperature measured in situ since the mid-nineteenth century: The HadSST2 dataset. *Journal of Climate*, 19(3), 446-469.
- Reason, C., 2001. Subtropical Indian Ocean SST dipole events and southern African rainfall. *Geophysical Research Letters*, 28(11), 2225-2227.
- Roxy, M.K., Ritika, K., Terray, P. and Masson, S., 2014. The curious case of Indian Ocean warming. *Journal of Climate*, 27(22), 8501-8509.
- Roxy, M.K. et al., 2015. Drying of Indian subcontinent by rapid Indian Ocean warming and a weakening land-sea thermal gradient. *Nature communications*, 6(1), 1-10.
- Sahany, S., Mishra, S.K. and Salunke, P., 2019. Historical simulations and climate change projections over India by NCAR CCSM4: CMIP5 vs. NEX-GDDP. *Theoretical and Applied Climatology*, 135(3-4), 1423-1433.

- Saji, N., Goswami, B., Vinayachandran, P. and Yamagata, T., 1999. A dipole mode in the tropical Indian Ocean. *Nature*, 401(6751), 360-363.
- Schlesinger, M.E. and Ramankutty, N., 1994. An oscillation in the global climate system of period 65–70 years. *Nature*, 367(6465), 723-726.
- Seow, M. X. C. (2018), A new type of tropical Pacific warming---El Niño Modoki, *Physics Today*, 71(12), 50-52.
- Sharmila, S., Joseph, S., Sahai, A., Abhilash, S. and Chattopadhyay, R., 2015. Future projection of Indian summer monsoon variability under climate change scenario: An assessment from CMIP5 climate models. *Global and Planetary Change*, 124, 62-78.
- Singh, D., Ghosh, S., Roxy, M.K. and McDermid, S., 2019. Indian summer monsoon: Extreme events, historical changes, and role of anthropogenic forcings. *Wiley Interdisciplinary Reviews: Climate Change*, 10(2), e571.
- Smith, T.M. and Reynolds, R.W., 2004. Improved extended reconstruction of SST (1854–1997). *Journal of climate*, 17(12), 2466-2477.
- Smith, T.M., Reynolds, R.W., Peterson, T.C. and Lawrimore, J., 2008. Improvements to NOAA's historical merged land–ocean surface temperature analysis (1880–2006). *Journal of Climate*, 21(10), 2283-2296.
- Solomon, A. et al., 2011. Distinguishing the roles of natural and anthropogenically forced decadal climate variability: implications for prediction. *Bulletin of the American Meteorological Society*, 92(2), 141-156.
- Stocker, T.F. et al., 2013. *Climate Change 2013. The Physical Science Basis. Working Group I Contribution to the Fifth Assessment Report of the Intergovernmental Panel on Climate Change-Abstract for decision-makers; Changements climatiques 2013. Les elements scientifiques. Contribution du groupe de travail I au cinquieme rapport d'evaluation du groupe d'experts intergouvernemental sur l'evolution du CLIMAT-Resume a l'intention des decideurs.*
- Sun, C. et al., 2019. Recent acceleration of Arabian Sea warming induced by the Atlantic-western Pacific trans-basin multidecadal variability. *Geophysical Research Letters*, 46(3), 1662-1671.
- Suzuki, R., Behera, S.K., Iizuka, S. and Yamagata, T., 2004. Indian Ocean subtropical dipole simulated using a coupled general circulation model. *Journal of Geophysical Research: Oceans*, 109(C9).
- Swanson, K.L., Sugihara, G. and Tsonis, A.A., 2009. Long-term natural variability and 20th century climate change. *Proceedings of the National Academy of Sciences*, 106(38), 16120-16123.
- Swapna, P., Krishnan, R. and Wallace, J., 2014. Indian Ocean and monsoon coupled interactions in a warming environment. *Climate dynamics*, 42(9-10), 2439-2454.
- Sweeney, C. et al., 2005. Impacts of shortwave penetration depth on large-scale ocean circulation and heat transport. *Journal of Physical Oceanography*, 35(6), 1103-1119.

- Takeuchi, E. and Yasuda, I., 2003. Wintertime shoaling of oceanic surface mixed layer. *Geophysical research letters*, 30(22).
- Thadathil, P., Suresh, I., Gautham, S., Prasanna Kumar, S., Lengaigne, M., Rao, R. R., ... & Hegde, A. (2016). Surface layer temperature inversion in the Bay of Bengal: Main characteristics and related mechanisms. *Journal of Geophysical Research: Oceans*, 121(8), 5682-5696.
- Tomita, H. and Kubota, M., 2011. Sampling error of daily mean surface wind speed and air specific humidity due to Sun-synchronous satellite sampling and its reduction by multi-satellite sampling. *International journal of remote sensing*, 32(12), 3389-3404.
- Trenberth, K.E. and Stepaniak, D.P., 2001. Indices of el niño evolution. *Journal of climate*, 14(8), 1697-1701.
- Vialard, J. and Delecluse, P., 1998. An OGCM study for the TOGA decade. Part I: Role of salinity in the physics of the western Pacific fresh pool. *Journal of Physical Oceanography*, 28(6), 1071-1088.
- Vidya, P., Ravichandran, M., Subeesh, M., Chatterjee, S. and Nuncio, M., 2020. Global warming hiatus contributed weakening of the Mascarene High in the Southern Indian Ocean. *Scientific reports*, 10(1), 1-9.
- Wang, C., Zou, L. and Zhou, T., 2018. SST biases over the Northwest Pacific and possible causes in CMIP5 models. *Science China Earth Sciences*, 61(6), 792-803.
- Wang, G., Cai, W., Yang, K., Santoso, A. and Yamagata, T., 2020. A unique feature of the 2019 extreme positive Indian Ocean Dipole event. *Geophysical Research Letters*, 47(18), e2020GL088615.
- Webster, P.J., Moore, A.M., Loschnigg, J.P. and Leben, R.R., 1999. Coupled ocean–atmosphere dynamics in the Indian Ocean during 1997–98. *Nature*, 401(6751), 356-360.
- Wild, M. et al., 2017. The Global Energy Balance Archive (GEBA) version 2017: A database for worldwide measured surface energy fluxes. *Earth System Science Data*, 9(2), 601-613.
- Wills, R.C., Schneider, T., Wallace, J.M., Battisti, D.S. and Hartmann, D.L., 2018. Disentangling global warming, multidecadal variability, and El Niño in Pacific temperatures. *Geophysical Research Letters*, 45(5), 2487-2496.
- Wu, L. et al., 2012. Enhanced warming over the global subtropical western boundary currents. *Nature Climate Change*, 2(3), 161-166.
- Wu, L. et al., 2012. Enhanced warming over the global subtropical western boundary currents. *Nature Climate Change*, 2(3), 161-166.
- Xie, S. P., Annamalai, H., Schott, F. A., & McCreary Jr, J. P. (2002). Structure and mechanisms of South Indian Ocean climate variability. *Journal of Climate*, 15(8), 864-878.
- Xie, S.P. and Kosaka, Y., 2017. What caused the global surface warming hiatus of 1998–2013? *Current Climate Change Reports*, 3(2), 128-140.

- Yeh, S.-W., Yim, B.Y., Noh, Y. and Dewitte, B., 2009. Changes in mixed layer depth under climate change projections in two CGCMs. *Climate dynamics*, 33(2-3), 199-213.
- Zazulie, N., M. Rusticucci, and G. B. Raga 2017), Regional climate of the subtropical central Andes using high-resolution CMIP5 models—Part I: Past performance (1980–2005), *Climate dynamics*, 49(11-12), 3937-3957.
- Zhang, L., Han, W., Karlsrukas, K.B., Meehl, G.A., Hu, A., Rosenbloom, N. and Shinoda, T., 2019. Indian Ocean warming trend reduces Pacific warming response to anthropogenic greenhouse gases: An interbasin thermostat mechanism. *Geophysical Research Letters*, 46(19), pp.10882-10890.
- Zheng, X.T., Xie, S.P., Lv, L.H. and Zhou, Z.Q., 2016. Intermodel uncertainty in ENSO amplitude change tied to Pacific Ocean warming pattern. *Journal of Climate*, 29(20), pp.7265-7279.

Figures

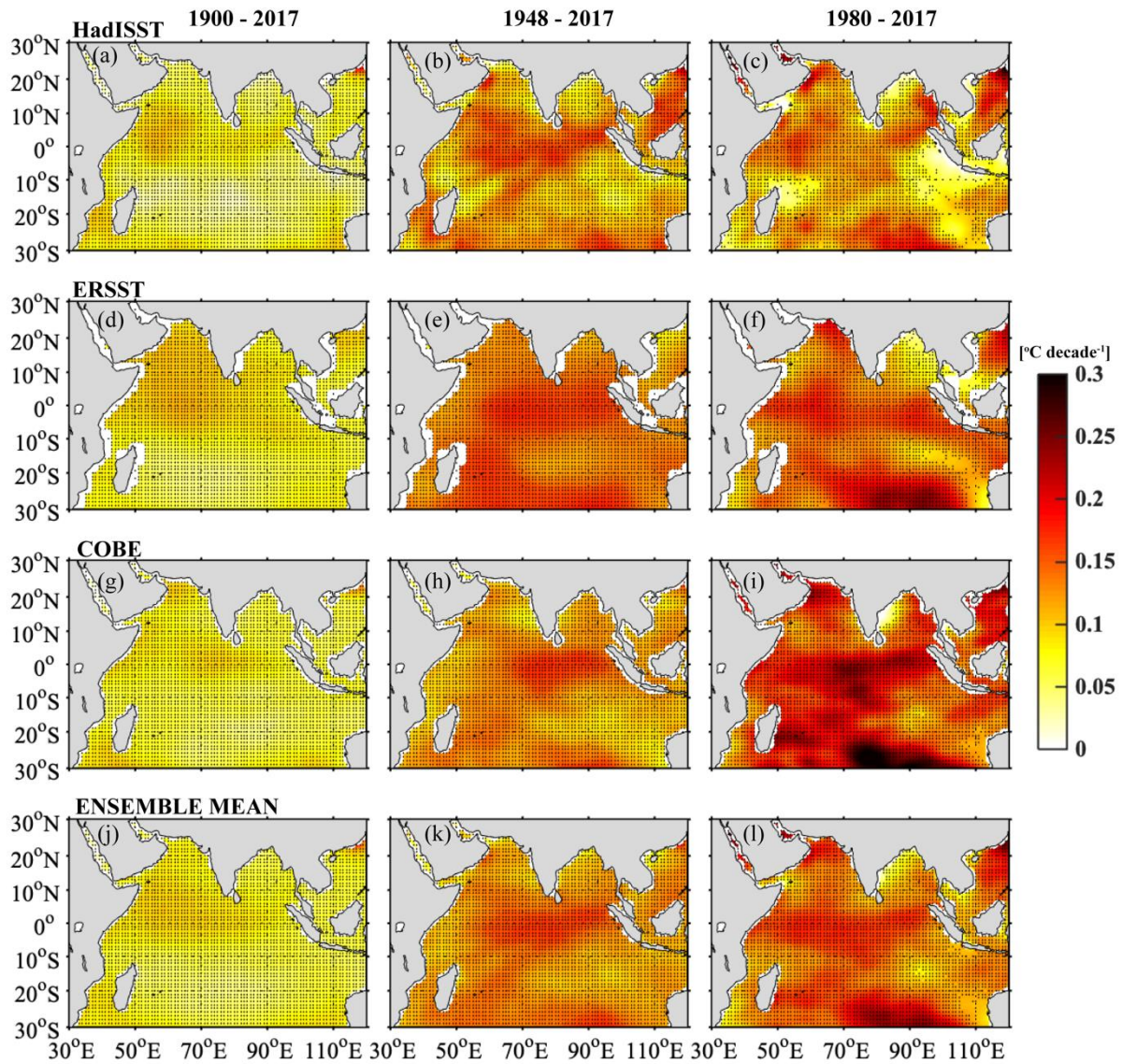


Figure 1. Linear long-term trends of SST in (a-c) HadISST, (d-f) ERSST, (g-i) COBE, and (j-l) their ensemble mean for the period 1900-2017 (left), 1948-2017 (middle), and 1980-2017 (right). Stipplings indicate the statistically significant trends at 95% confidence level based on Mann-Kendall test.

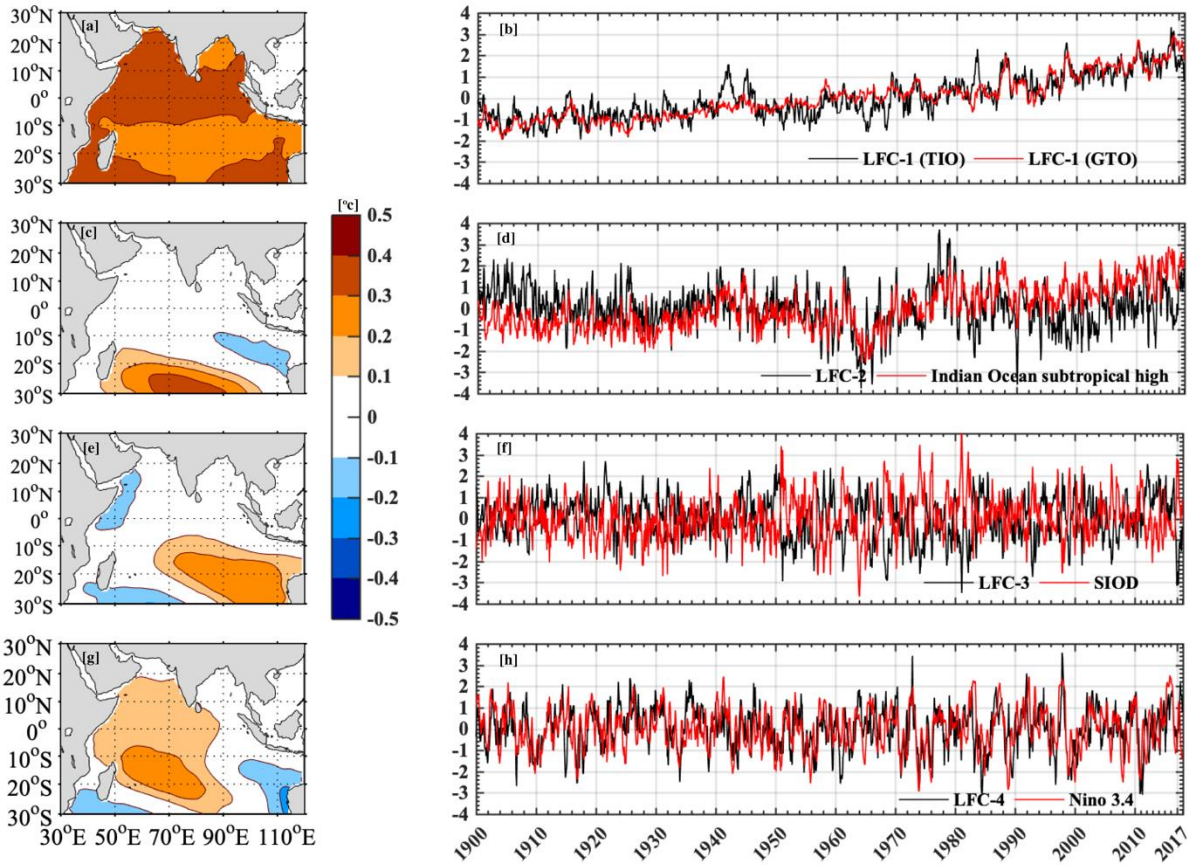


Figure 2. First four low frequency patterns (LFPs) and components (LFCs) of ensemble mean SST anomalies over the Tropical Indian Ocean region. LFC 1 is shown along with that of global tropical oceans and LFC 2 is shown with normalized SST anomalies averaged over the Indian Ocean subtropical high region (45°E–100°E and 20°S–40°S). The normalised SIOD and Niño3.4 indices are shown along with LFC 2 and LFC 4, respectively.

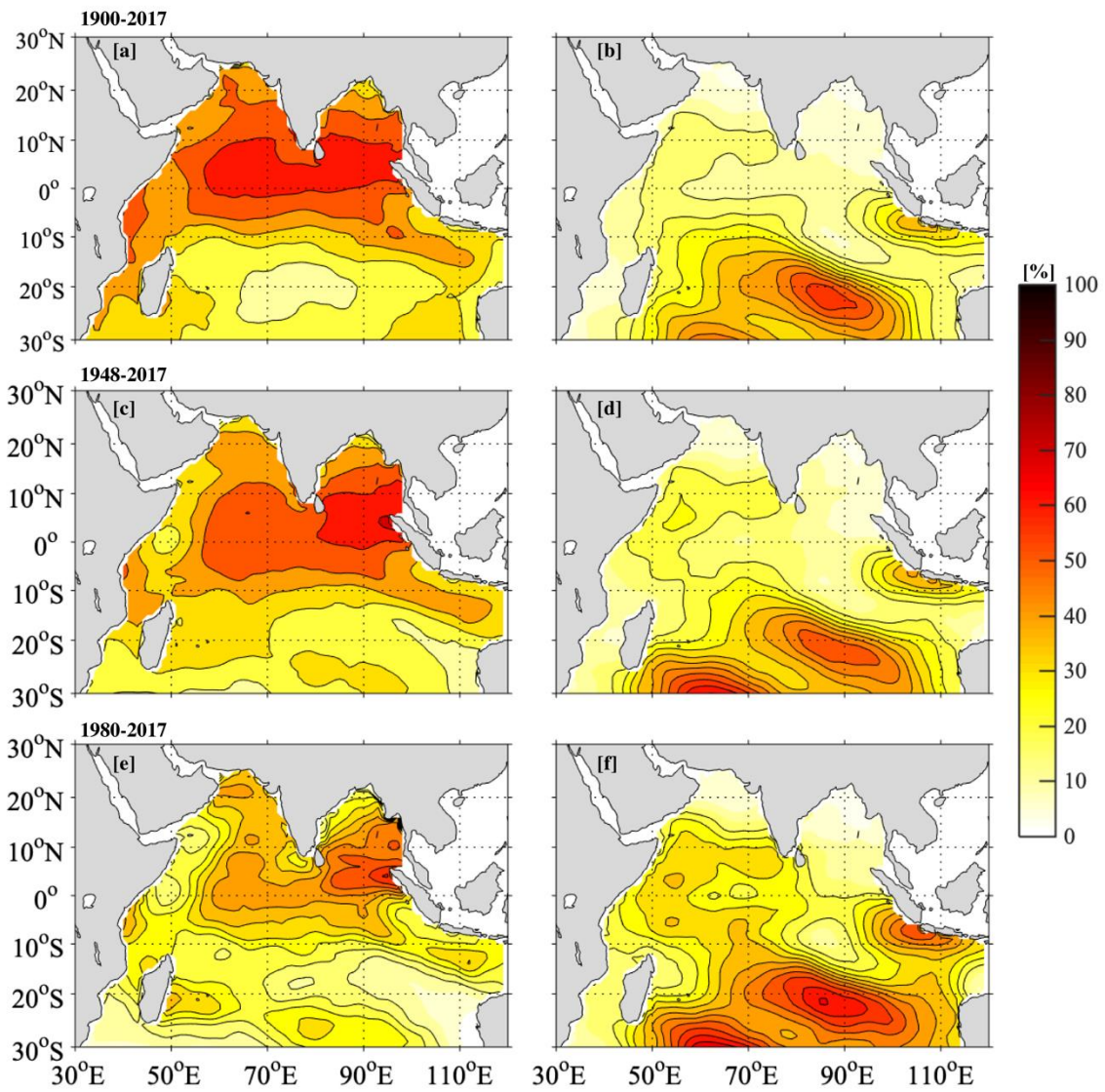


Figure 3. Total SST variance in each grid points of TIO explained by global warming signal (left) and climate modes (right) for the periods (a&b)1900-2017, (c&d) 1947-2017, and (e&f) 1980-2017.

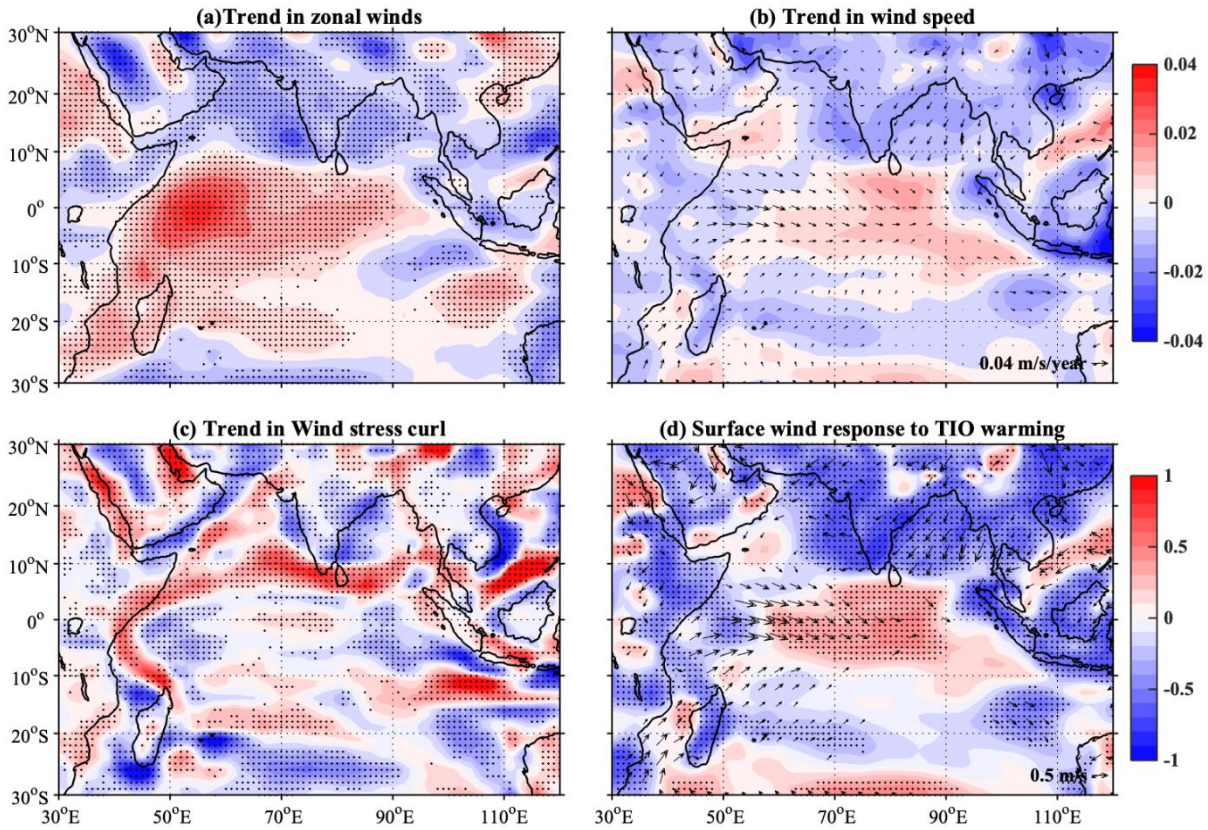


Figure 4. (a) Trend in surface zonal wind velocity (NCEP, 1948-2017, ms^{-1}). (b) Trend in surface wind speed (shading; ms^{-1}) and velocity (vectors; ms^{-1}). (c) Trend in surface wind stress curl (10^{-9}Nm^{-3}). Statistically significant trend values at 95% confidence level are highlighted by stippling. (d) Surface wind response (ms^{-1}) to tropical Indian Ocean warming. Shade indicates the spatial correlation pattern of wind speed with Indian Ocean warming signal. Vectors are obtained by regressing Indian Ocean warming signal onto zonal and meridional wind velocities. The vectors and stippling are shown over the regions where the regression and correlation coefficients respectively are statistically significant at 95% confidence level.

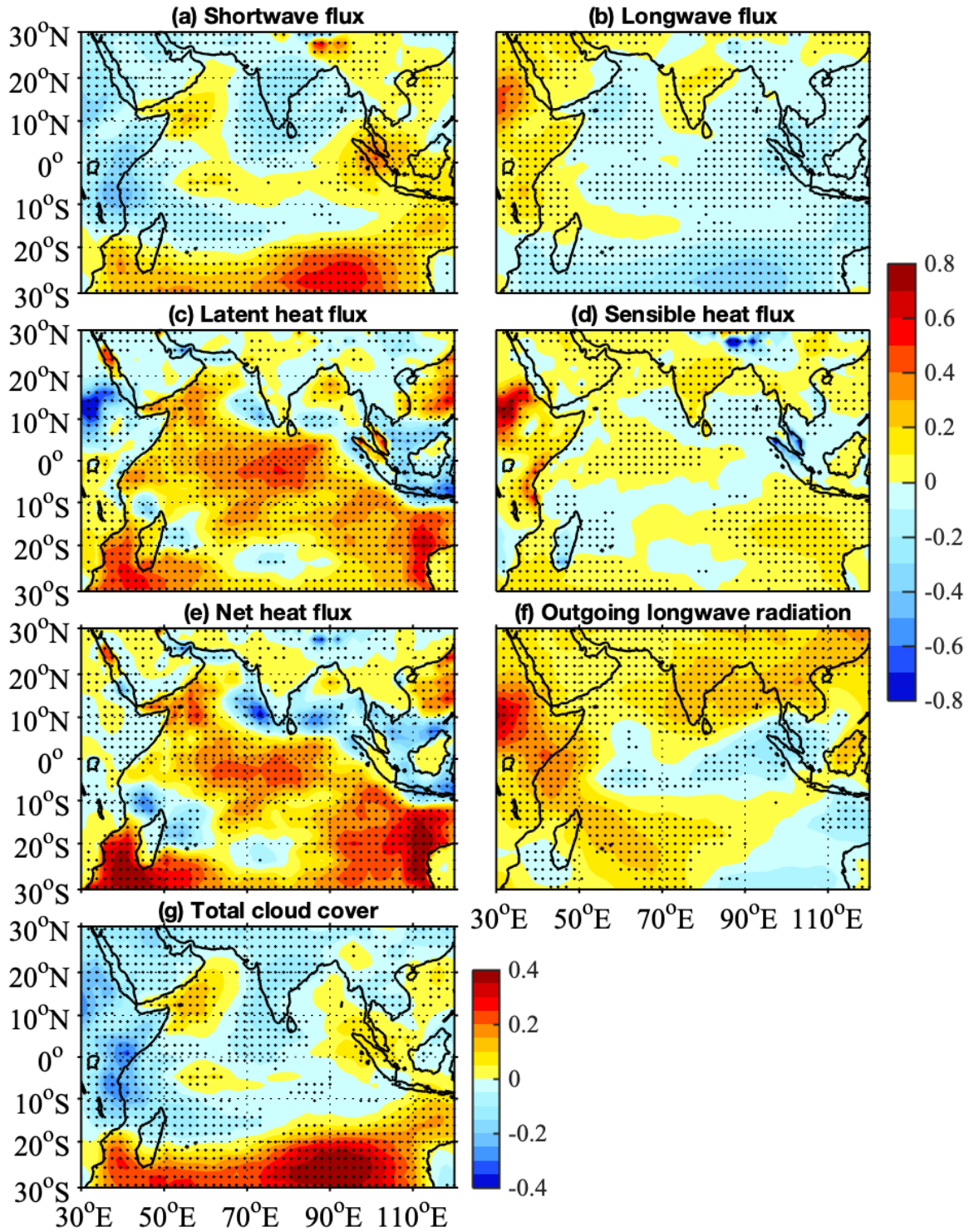


Figure 5. Trends in surface heat fluxes, OLR at the nominal top of the atmosphere and total cloud cover for the period 1948-2017. The sign conventions of fluxes are that the positive value indicates flux out of the ocean. Stipplings indicate the trends are statistically significant at 95% confidence level.

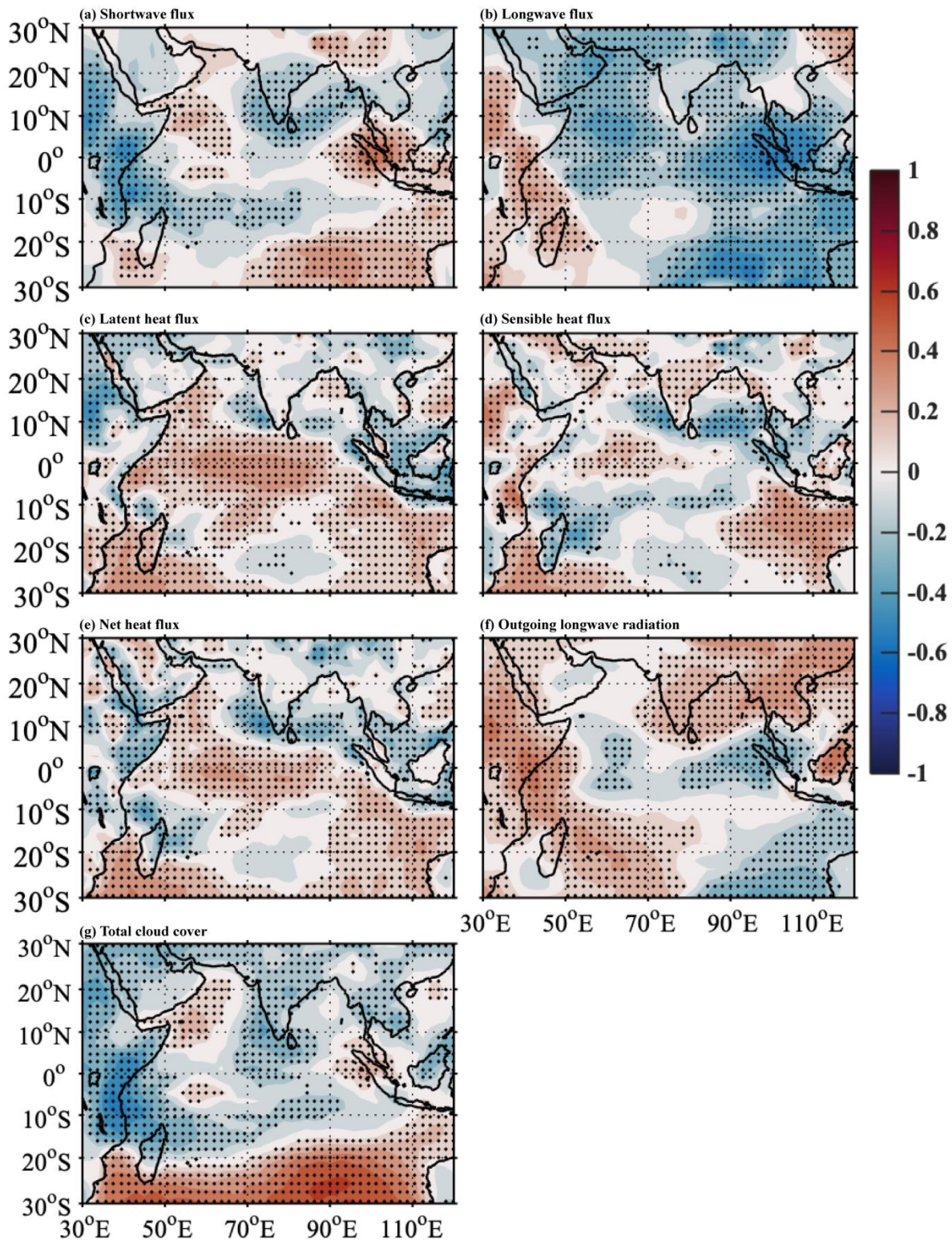


Figure 6. Correlation patterns of Indian Ocean warming signal and (a) net surface shortwave radiation flux, (b) net surface longwave radiation flux, (c) latent heat flux, (d) sensible heat flux, (e) net heat flux, (f) outgoing longwave radiation at the top of the atmosphere and (d) total cloud cover for the period 1948-2017. Black dots indicate the regions where correlation coefficients are statistically significant at 95% confidence level.

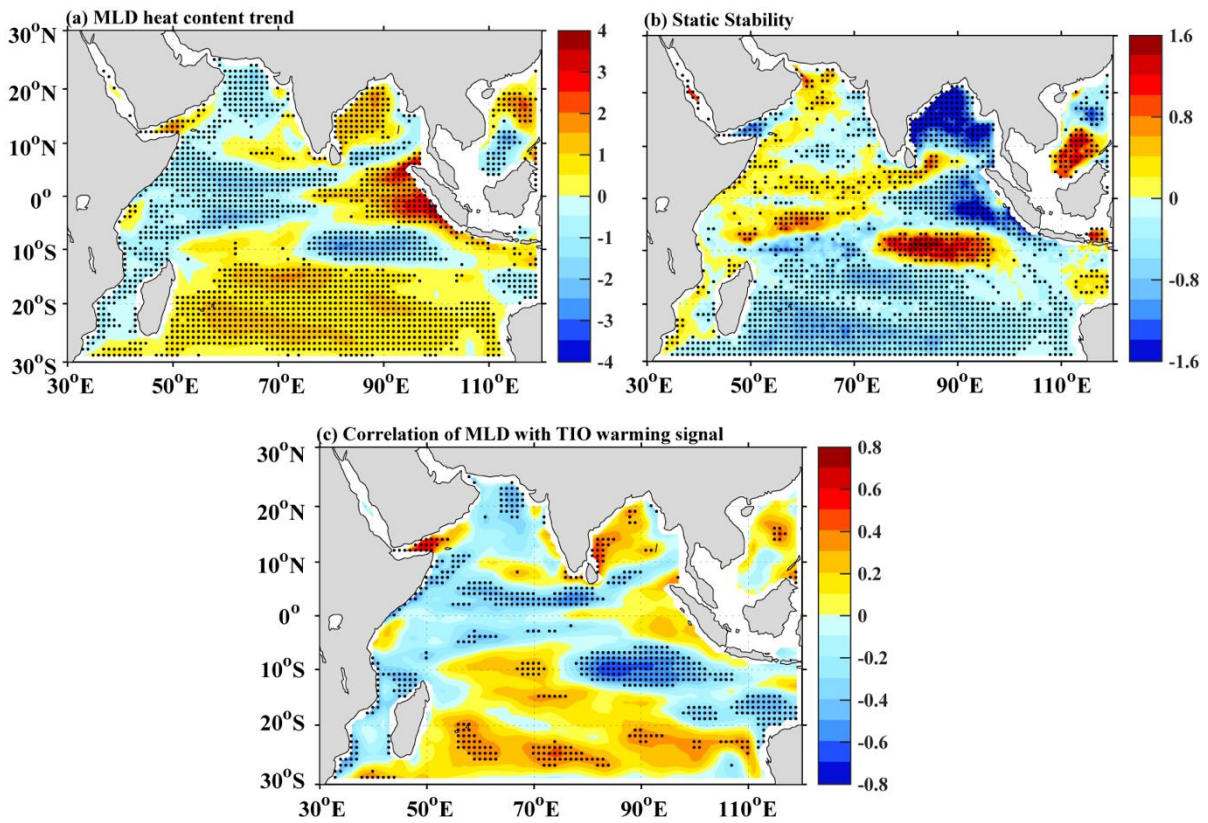


Figure 7. (a) Linear trend ($10^7 \text{ Jm}^{-2} \text{ year}^{-1}$) of mixed layer heat content, (b) linear trend of mixed layer static stability ($10^{-5} \text{ m}^{-1} \text{ year}^{-1}$) and (c) correlation pattern of TIO warming signal with MLD. Stippling denotes the statistically significant value of linear trend and correlation coefficient at 95% level.

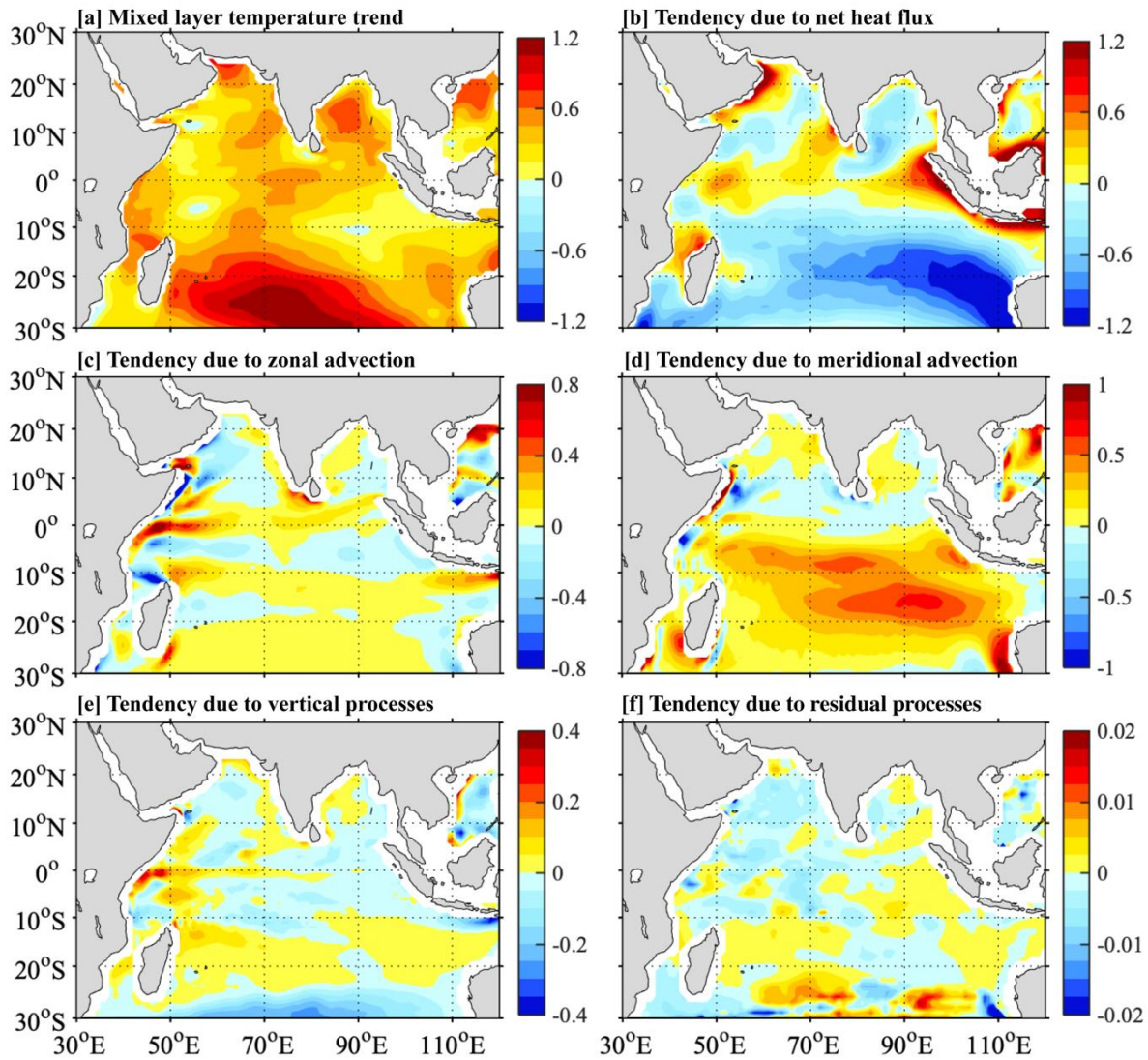


Figure 8. (a) Long-term trend of temperature averaged over the mixed layer and temperature change ($^{\circ}\text{C } 38\text{year}^{-1}$) contributed by (b) net heat flux, (c) zonal advection, (d) meridional advection, (e) vertical processes, and (f) residual components of mixed layer heat budget computed for the period 1980-2017.

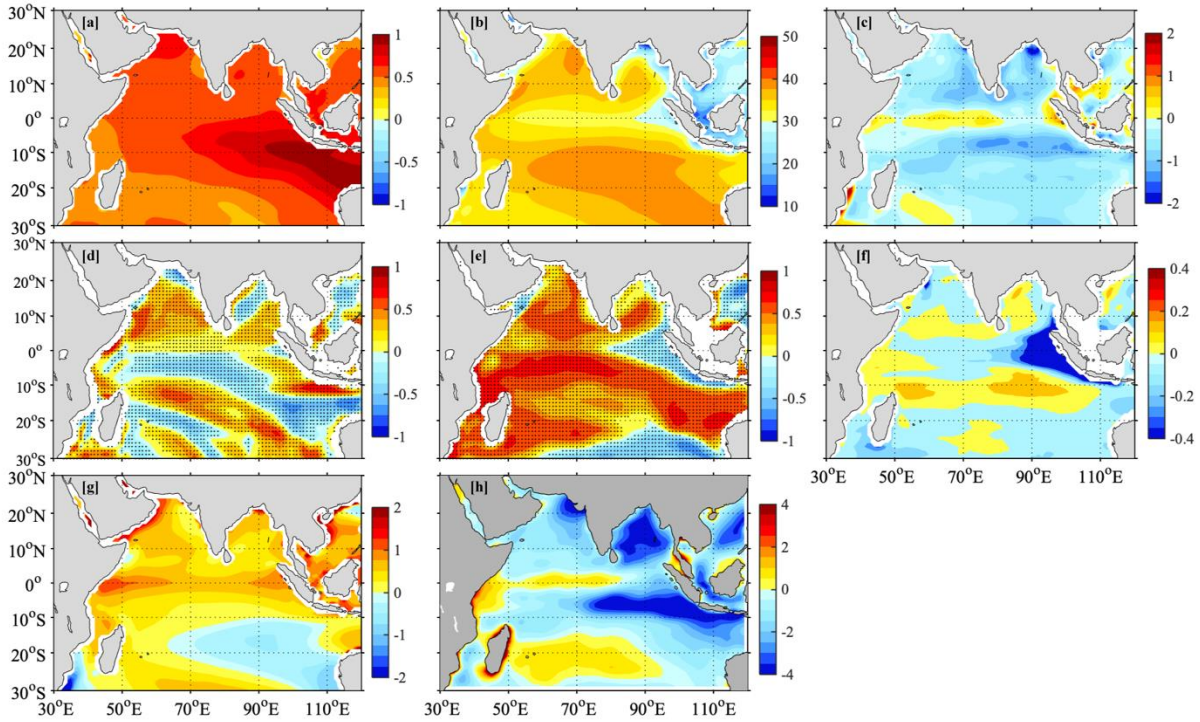


Figure 9. Temperature and mixed layer processes simulated by CESM2 historical simulation for the period 1900-2014. (a) Long-term trend of temperature averaged over the mixed layer ($^{\circ}\text{C } 115\text{year}^{-1}$). (b) Mixed layer depth climatology (m) and (c) long-term trend ($\text{m } 115\text{year}^{-1}$). Pointwise correlation pattern of mixed layer temperature tendency anomalies with (d) horizontal advection and (e) vertical advection anomalies. Stipplings denote the statistically significant correlation values at 95% confidence level. Mixed layer temperature tendency ($^{\circ}\text{C } 115\text{year}^{-1}$) due to (f) vertical processes and (g) net heat flux. (h) Long-term trend of surface wind speed ($\text{ms}^{-1} 115\text{year}^{-1}$) in CESM2 historical simulation for the same period.